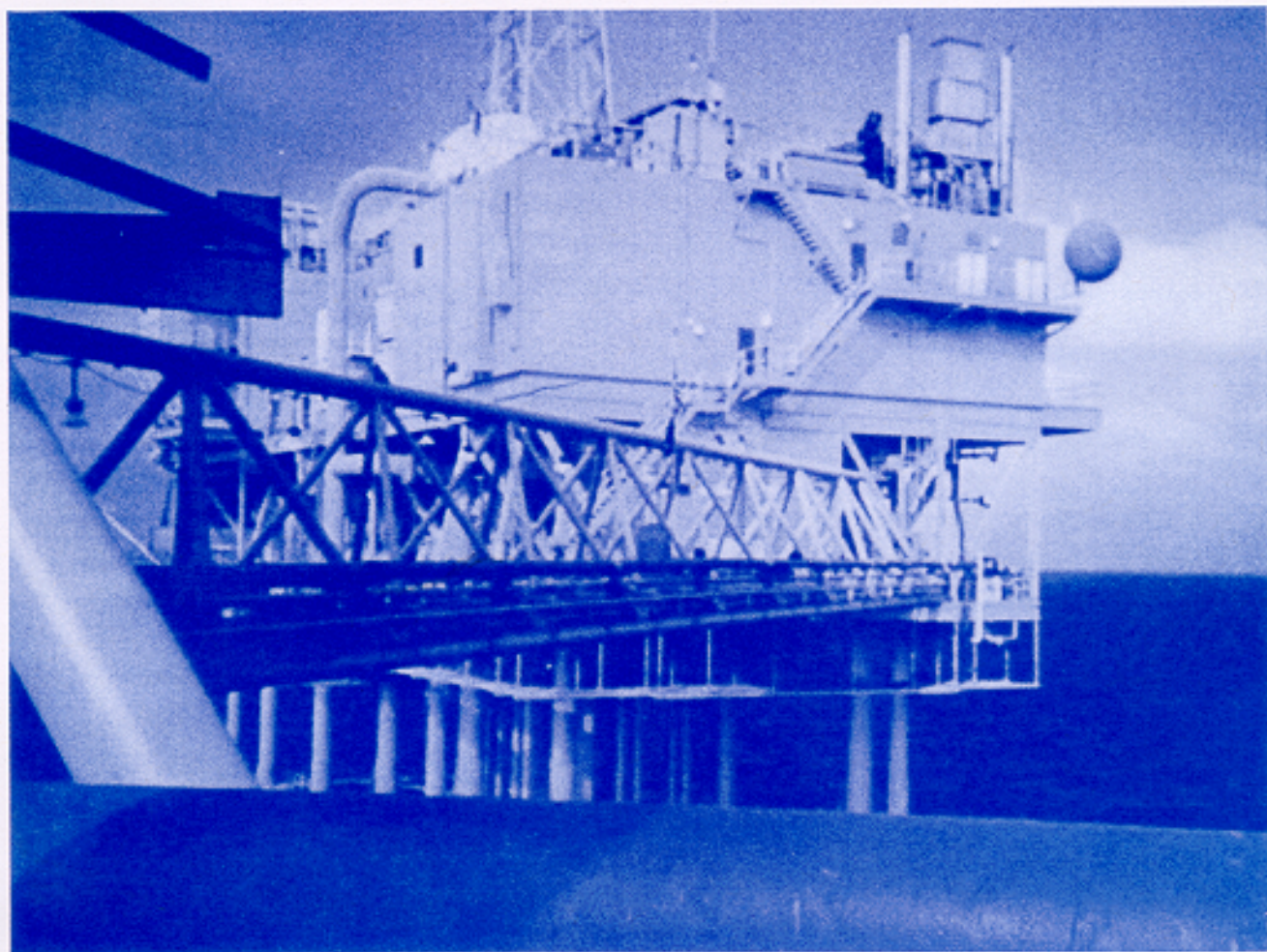# A Fatigue Model for Fiber-Reinforced Polymeric Composites for Offshore Applications

Tinh Nguyen, Hai Tang, Tze-jer Chuang, Joannie Chin, Felix Wu, and Jack Lesko

NIST

National Institute of Standards and Technology
Technology Administration, U.S. Department of Commerce

NIST CENTENNIAL
1901-2001

*T*he National Institute of Standards and Technology was established in 1988 by Congress to "assist industry in the development of technology . . . needed to improve product quality, to modernize manufacturing processes, to ensure product reliability . . . and to facilitate rapid commercialization . . . of products based on new scientific discoveries."

NIST, originally founded as the National Bureau of Standards in 1901, works to strengthen U.S. industry's competitiveness; advance science and engineering; and improve public health, safety, and the environment. One of the agency's basic functions is to develop, maintain, and retain custody of the national standards of measurement, and provide the means and methods for comparing standards used in science, engineering, manufacturing, commerce, industry, and education with the standards adopted or recognized by the Federal Government.

As an agency of the U.S. Commerce Department's Technology Administration, NIST conducts basic and applied research in the physical sciences and engineering, and develops measurement techniques, test methods, standards, and related services. The Institute does generic and precompetitive work on new and advanced technologies. NIST's research facilities are located at Gaithersburg, MD 20899, and at Boulder, CO 80303. Major technical operating units and their principal activities are listed below. For more information contact the Publications and Program Inquiries Desk, 301-975-3058.

Office of the Director
- National Quality Program
- International and Academic Affairs

Technology Services
- Standards Services
- Technology Partnerships
- Measurement Services
- Information Services

Advanced Technology Program
- Economic Assessment
- Information Technology and Applications
- Chemistry and Life Sciences
- Materials and Manufacturing Technology
- Electronics and Photonics Technology

Manufacturing Extension Partnership Program
- Regional Programs
- National Programs
- Program Development

Electronics and Electrical Engineering Laboratory
- Microelectronics
- Law Enforcement Standards
- Electricity
- Semiconductor Electronics
- Radio-Frequency Technology[1]
- Electromagnetic Technology[1]
- Optoelectronics[1]

Materials Science and Engineering Laboratory
- Intelligent Processing of Materials
- Ceramics
- Materials Reliability[1]
- Polymers
- Metallurgy
- NIST Center for Neutron Research

Chemical Science and Technology Laboratory
- Biotechnology
- Physical and Chemical Properties[2]
- Analytical Chemistry
- Process Measurements
- Surface and Microanalysis Science

Physics Laboratory
- Electron and Optical Physics
- Atomic Physics
- Optical Technology
- Ionizing Radiation
- Time and Frequency[1]
- Quantum Physics[1]

Manufacturing Engineering Laboratory
- Precision Engineering
- Automated Production Technology
- Intelligent Systems
- Fabrication Technology
- Manufacturing Systems Integration

Building and Fire Research Laboratory
- Applied Economics
- Structures
- Building Materials
- Building Environment
- Fire Safety Engineering
- Fire Science

Information Technology Laboratory
- Mathematical and Computational Sciences[2]
- Advanced Network Technologies
- Computer Security
- Information Access and User Interfaces
- High Performance Systems and Services
- Distributed Computing and Information Services
- Software Diagnostics and Conformance Testing
- Statistical Engineering

---

[1] At Boulder, CO 80303.
[2] Some elements at Boulder, CO.

NIST Technical Note 1434

A Fatigue Model for Fiber-Reinforced Polymeric Composites for Offshore Applications

Tinh Nguyen[1], Hai Tang[2], Tze-jer Chuang[3], Joannie Chin[1], and Felix Wu[4]
[1]Building Materials Division, Building and Fire Research Laboratory
[2]High Performance Systems and Services Division, Information Technology Laboratory
[3]Ceramics Division, Materials Science and Engineering Laboratory
[4]Chemistry and Life Sciences Office, Advanced Technology Program
National Institute of Standards and Technology
Gaithersburg, MD 20899-8113

Jack Lesko
Virginia Polytechnic Institute and State University
Blacksburg, VA 24061

September 2000

Table of Contents

A Model for Predicting the Fatigue Life of Fiber-Reinforced Polymeric Composites in Offshore Applications

Tinh Nguyen, Hai Tang, Tze-jer Chuang, Joannie Chin, Felix Wu, and Jack Lesko*

National Institute of Standards and Technology, Gaithersburg, MD 20899

*Virginia Polytechnic Institute and State University, Blacksburg, VA 24061

ABSTRACT

A model based on cumulative damage has been developed for predicting the fatigue life of fiber-reinforced polymeric composites used in offshore environments. The model incorporates applied stress, stress amplitude, loading frequency, residual tensile modulus, and material constants as parameters. The model is verified with experimental data from a glass fiber/vinyl ester composite fatigued under different environmental conditions. Specimens are subjected to tension-tension fatigue at four levels of applied maximum tensile stress at two different frequencies while exposed to air, fresh water, and sea water at 30 °C. Both the residual mechanical properties at specified loading cycles and the number of cycles at which the specimens fail are measured. For the material used in this study, the loss in mechanical properties (residual tensile strength and modulus) in salt water is approximately the same as that in fresh water, and the fatigue life of the composite in these aqueous environments is shorter than that in air. The S-N curves for specimens subjected to the three environments have approximately the same slope, suggesting that the failure mechanism does not change with these environments. Furthermore, specimens that are fatigued at a lower frequency failed at a lower number of cycles than those tested at a higher frequency. Numerical analysis is performed using the fatigue experimental data to determine the material constants of the composite. The model agrees well with the experimental data, and it can be used to predict the fatigue life of polymeric composites subjected to an applied load in different environments or the residual tensile modulus after a number of loading cycles.

INTRODUCTION

Over the last three decades, fiber-reinforced polymer (FRP) composites have been used extensively in a wide range of aerospace and military applications. There is a growing interest in extending the use of these materials into civil engineering structures such as offshore platforms [1,2]. An urgent need exists to develop quantitative analysis and methodology for assessing the safety and reliability of using polymer composites in these applications. One particularly critical issue in regard to using polymer composites in structural applications is their fatigue reliability in different environments and loading conditions. Fatigue damage in polymer composites for non-civil engineering applications has been extensively investigated [3-7]. Studies of the effects of water or salt water on the fatigue behavior of polymer composites have also been widely reported [8-14]. However, there is little quantitative research on the effects of civil engineering environments, namely water, sea water, concrete pore solution, temperature, ultraviolet radiation, and loading on the fatigue of polymeric composites. The main objective of this study is to develop experimentally verifiable models for predicting the fatigue life of polymer composites used in civil engineering structures.

This report presents the development of a fatigue model, results of the fatigue experiments for a glass fiber/vinyl ester composite subjected to different loading and environmental conditions, and the verification of the model. The model can be used to predict fatigue life of polymeric composites under an applied load and to estimate the residual tensile modulus after a certain number of loading cycles.

DERIVATION OF FATIGUE MODEL FOR FIBER-REINFORCED POLYMER COMPOSITES FOR OFFSHORE APPLICATIONS

Fatigue Model

The basic failure mechanisms most commonly observed in fatigue of fiber-reinforced polymer composites are matrix cracking, fiber-matrix debonding, ply delamination, and fiber breakage [3,4,15-18]. Cumulative damage as a function of loading cycles may be generally described by the curve given in Figure 1, where D represents cumulative damage, N is the

number of loading cycles, and N_f is the number of cycles to failure. The change in material modulus has been commonly used to express the state of damage in polymer composites [3,15,16,19]. In this work, cumulative damage, D, is defined as:

$$D = 1 - \frac{E}{E_0} \qquad (1)$$

where E and E_0 are the residual and initial moduli, respectively. For typical multidirectional laminate polymer composites, matrix cracks are initiated early in the fatigue process due to high stress concentrations. As the crack density increases, stress redistribution limits the initiation of new cracks. At this stage, the damage appears to grow at a constant rate as the cyclic loading continues. In the region of damage, fiber/matrix interfacial debonding, delamination of the laminates, and fiber breakage begin to occur and gradually increase. As the fiber breakage progresses and intensifies, the rate of fiber fracture increases rapidly and, finally, the composite ruptures.

The incremental damage per loading cycle, dD/dN, as a function of cumulative damage, D, which may be derived from Figure 1, is displayed in Figure 2. The initial damage growth per loading cycle may be mathematically expressed in either of the following two functions:

$$\frac{dD}{dN} = \frac{C_1}{D^{n_1}} \qquad (2)$$

or

$$\frac{dD}{dN} = B_1 e^{-n_1 D} \qquad (3)$$

where N is the number of loading cycles, and C_1 and B_1 and n_1 are constants with $n_1 > 1$.
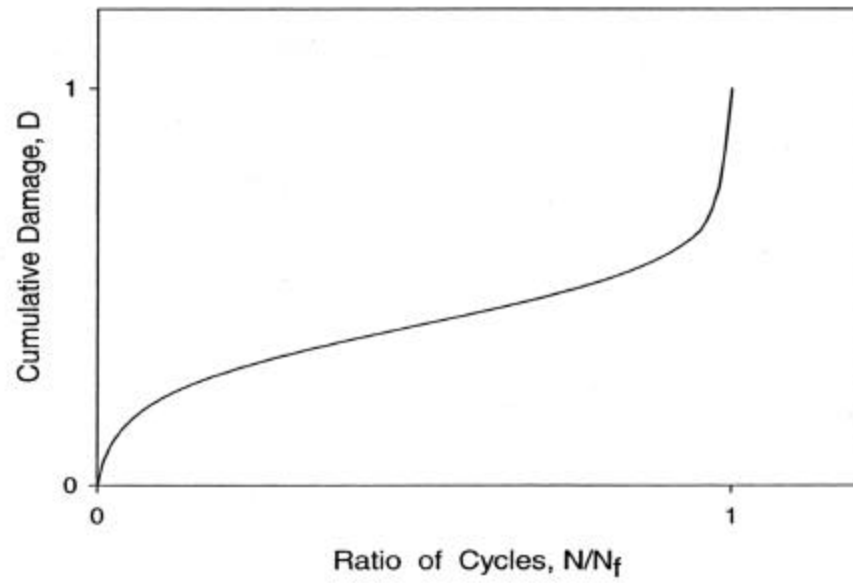
Figure 1: Cumulative damage, D, as a function of the ratio of the number of loading cycles, N, to the number of cycles at failure, N_f.
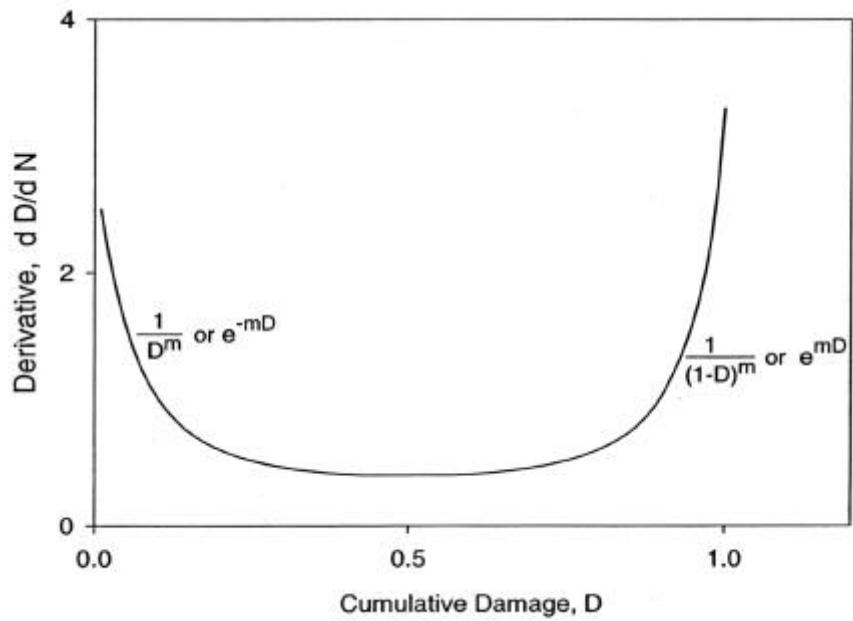

Figure 2: Damage growth as a function of cumulative damage.

The damage growth rate near the end of the life cycle before failure may be described by:

$$\frac{dD}{dN} = \frac{C_2}{(1-D)^{n_2}}$$ (4)

or

$$\frac{dD}{dN} = B_2 e^{n_2 D}$$ (5)

where B_2, C_2 and n_2 are constants and $n_2 > 1$.

The general fatigue model as depicted in Figure 2 may take the form:

$$\frac{dD}{dN} = \frac{C_1}{D^{n_1}} + \frac{C_2}{(1-D)^{n_2}}$$ (6)

or

$$\frac{dD}{dN} = B_1 e^{-n_1 D} + B_2 e^{n_2 D}$$ (7)

However, our experimental data on the cumulative damage, D, as a function of the number of loading cycles, N, for a glass fiber/vinyl ester composite do not show any initial strength degradation until the number of loading cycles exceeds 1000. Further, the initial damage does not reveal any evidence of an abrupt growth phenomenon (see, e.g. Figure 12). Instead, the normalized modulus data shows smooth, gradual decrease from the undamaged state. Therefore, for this composite material, C_1 is negligible in comparison with C_2. Consequently, the damage rate per loading cycle may be expressed by the following function:

$$\frac{dD}{dN} = \frac{C}{(1-D)^n}$$ (8)

or

$$\frac{dD}{dN} = B e^{nD}$$ (9)

5

where B, C and n are again material constants. In Figure 3, the curves represented by Eq. 8 and Eq. 9 are compared with B = C = 1. From this figure, Eq. 8 appears to better represent the sudden rupture of the composite material as D approaches unity. Therefore, Eq. 8 will be expanded to describe the fatigue process for vinyl ester/E-glass fiber composites used in civil engineering applications.

Figure 3: Comparison between damage growth as a function of exponential damage and inverse exponential damage for different values of n.

Besides the state of damage, the maximum stress and stress amplitude may also have substantial effects on the damage growth. Accordingly, Eq. 8 may be rewritten as:

$$\frac{dD}{dN} = C_o \frac{(\sigma_{max} \sigma_{amp})^m}{(1-D)^n} \tag{10}$$

where

C_o, m and n are the material constants,

σ_{max} is the maximum stress,

σ_{min} is the minimum stress, and

σ_{amp} is the cyclic stress amplitude and is equal to (σ_{max} - σ_{min})

We can express the maximum stress and stress amplitude in normalized terms with respect to the ultimate tensile strength (σ_{ult}) and the minimum to maximum stress ratio R:

$$S_{max} = \frac{S_{max}}{S_{ult}} \tag{11}$$

$$S_{amp} = \frac{S_{amp}}{S_{ult}} = \frac{S_{max} - S_{min}}{S_{ult}} = \frac{S_{max}}{S_{ult}}(1 - \frac{S_{min}}{S_{max}}) = S_{max}(1 - R) \tag{12}$$

Substituting for σ_{max} and σ_{amp} in Eq. 10 and then simplifying, the equation becomes:

$$\frac{dD}{dN} = C\ \frac{(S^2_{max}(1-R))^m}{(1-D)^n} \tag{13}$$

where $|S_{max}| \leq 1$ and $C = C_o(\sigma_{ult})^{2m}$.

Integrating Eq. 13 and substituting the initial condition, i.e., D = 0 when N = 0, we obtain:

$$\frac{1}{n+1} - \frac{(1-D)^{n+1}}{n+1} = C(S^2_{max}(1-R))^m N \tag{14}$$

where $0 \leq D \leq 1$.

When the number of loading cycles approaches the maximum number of cycles N_f, D approaches 1. Under this condition, Eq. 14 becomes:

$$\frac{1}{n+1} = C(S^2_{max}(1-R))^m N_f \tag{15}$$

Eq. 15 is equivalent to the power formula often seen in the literature as:

$$s_{max}^{A} N_f = \text{constant} \qquad (16)$$

which can also be expressed as:

$$\log s_{max} = -\frac{1}{A} \log N_f + \text{constant} \qquad (17)$$

where A is a constant.

In the model validation section, this equation will be compared with the following expression:

$$s_{max} = m \log N_f + \text{constant} \qquad (18)$$

which is commonly used for characterizing fatigue life, N_f, of materials.

Determination of the Material Constants

The constants m, n, and C in Eqs. 14 and 15 can be obtained if experimental fatigue data of polymer composites are available. This section describes the methods for determining these constants.

Taking the logarithm of both sides of Eq. 15, we obtain:

$$\log[(n+1)C] + 2m \log(S_{max}) + m \log(1-R) + \log N_f = 0 \qquad (19)$$

Therefore, the linear regression slope (-1/2m) of the S_{max} versus N_f plot in log-log scale can be used to compute the material constant m.

To determine the value of n, we need to use the solution in the intermediate state with partial damage D in Eq. 14. Since D is usually small until it approaches the maximum number of life cycles, we can expand the $(1-D)^{n+1}$ term with a Taylor's series and omit the higher order terms. Accordingly, Eq. 14 becomes:

$$\frac{1}{n+1}\left[1 - 1 + (n+1)D - \frac{(n+1)n}{2!}D^2 + \ldots\right] = C(S_{max}^2(1-R))^m N \qquad (20)$$

8

For the same applied load where the residual modulus is measured at two different numbers of cycles N_1 and N_2, the respective damages D_1 and D_2 can be computed, and Eq. 20 gives:

$$D_1(1-\frac{n}{2}D_1) = C(S_{max}^2(1-R))^m N_1 \qquad (21)$$

$$D_2(1-\frac{n}{2}D_2) = C(S_{max}^2(1-R))^m N_2 \qquad (22)$$

Dividing Eq. 21 by Eq. 22 and canceling the common terms, we have:

$$\frac{D_1(1-\frac{n}{2}D_1)}{D_2(1-\frac{n}{2}D_2)} = \frac{N_1}{N_2} \qquad (23)$$

or

$$(1-\frac{n}{2}D_1) = \frac{N_1}{N_2}\frac{D_2}{D_1}(1-\frac{n}{2}D_2) = K_{12}(1-\frac{n}{2}D_2) \qquad (24)$$

where

$$K_{12} = \frac{N_1}{N_2}\frac{D_2}{D_1} \qquad (25)$$

Therefore,

$$n = \frac{2(1-K_{12})}{(D_1-D_2K_{12})} \qquad (26)$$

The remaining parameter C can then be determined using the plot of maximum stress versus the number of cycles at failure (S-N curve) in Eq. 15 and the previously determined m and n values.

It should be noted that the material constants, C, m, and n could be dependent on the fatigue frequency. However, as will be shown in the following section, our experimental data for

9

two frequencies, 2 Hz and 10 Hz, indicate that frequency has little effect on m or n, but it has a substantial effect on C.

EXPERIMENTAL PROCEDURE[1]

Materials

The specimens used for this study were obtained from a pultruded vinyl ester/E-glass fiber composite supplied by Strongwell (Bristol, VA). The composite is similar to the material used in the construction of the Tom's Creek composite bridge in Blacksburg, VA. The flat laminate was constructed from unidirectional roving and continuous strand mat. The fiber volume fraction was approximately 28 % to 30 %, as determined by combustion of the matrix. Coupons having dimensions of 22.9 cm long x 2.54 cm wide x 0.32 cm thick were cut from a 40.6 cm x 122 cm plate. The edges of the specimen were sanded to ensure uniformity and were coated with a filled epoxy material to minimize the sorption of exposure solution into the composite from the edges.

Preparation of Test Solution

A solution containing 3.5 % mass fraction of NaCl in distilled water was used to simulate sea water. To ensure that all specimens were exposed to approximately the same salt concentration, a fresh solution was used for each batch of specimens. In addition, the salinity of the solution was monitored by a salimeter and adjusted by adding fresh solution. A calibration curve was generated for 1 % and 4 % mass fraction of NaCl, and the concentration was plotted against their corresponding volume displacements, as measured by the salimeter. Subsequent measurements were checked against these established conditions.

---

[1] Certain commercial materials and equipment are identified in this paper in order to specify adequately the experimental procedure. In no case does such identification imply recommendation or endorsement by the National Institute of Standards and Technology (NIST), nor does it imply that they are necessarily the best available for the purpose.

Fluid Cell

A transparent fluid cell was designed to hold the salt solution and water around the specimens during the fatigue experiment. Figure 4 displays a typical fluid cell assembly with a test specimen in place. The fluid cell consisted of two poly(methylmethacrylate) (PMMA) plates. Each of the plates had a groove to hold the specimen and a central depression to contain the solution during cycling. Six screws were used to fasten the two plates together, enclosing the mid-section of the specimen. Silicone sealant was laid along the edges of the depression to prevent leaking during testing. In most cases, the fluid did not leak from the cell during cycling, but only when the specimen failed.
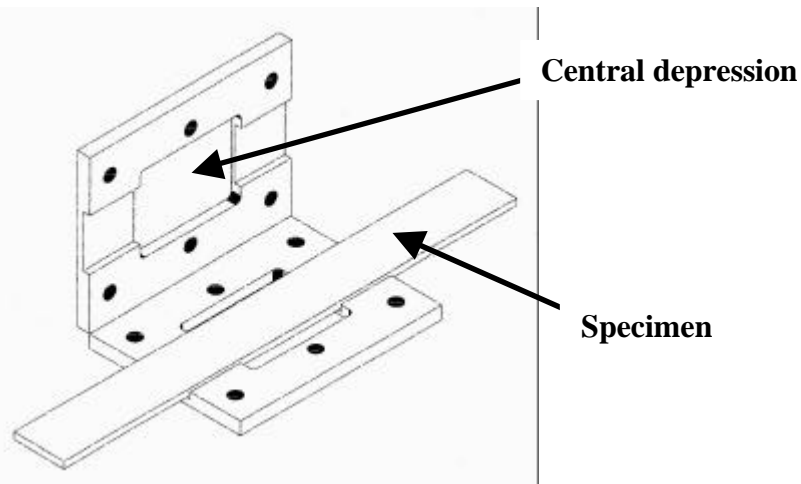

Figure 4: Fluid cell assembly used for fatigue testing of polymer composite in simulated sea water at a specified temperature.

Procedure for Saturation of Specimens in Simulated Sea Water at 65 °C

All composite specimens used for fatigue measurement in water and simulated sea water were presaturated with the respective solutions at 65 °C. This elevated temperature was used to accelerate the diffusion of solutions into the composite. Equipment used for the saturation consisted of a 76-liter tank made of transparent glass to facilitate experimental monitoring without disturbing the setup. Four aquarium heaters were mounted at four corners of the tank. A temperature controller was used to maintain the temperature at 65 °C. Two power pumps were

placed in the tank to ensure uniform heat distribution in the solution during aging. The tank was insulated to reduce evaporation and heat loss.

Edge-coated specimens were individually weighed before placing them into the saturation tank. Specimens were carefully arranged on a rack to ensure a uniform exposure of each specimen to the solution. The mass uptake of each specimen was measured daily by removing it from the tank, blotting, weighing, and placing it back in the tank. The result was the average of seven specimens.

Percent mass uptake was computed as follows:

$$\% \ M = \left(\frac{M_2 - M_1}{M_1} \right) x \, 100 \qquad (27)$$

Where: % M = percent mass uptake

M_1 = dry mass

M_2 = mass at specified time of immersion in solution

Specimen Preparation for Fatigue Test

Specimens were prepared by enclosing the central portion of the specimen within the fluid cell (see Figure 4). The remaining equal lengths on either side of the cell were used for gripping. A length of 12.5 mm was left between the cell and the grips of the testing machine on either side of the cell. Thus, a length of 50 mm of the specimen resided in the grips. Specimen ends were wrapped with fine wire mesh to prevent slippage within the grip areas during testing. As indicated earlier, six screws were used to fasten the two PMMA plates together and silicone sealant was used along the edges of the cell depression to seal the cell during fatiguing. Prepared specimens were stored for approximately 6 h to allow the silicone to cure before fatigue cycling began.

Measurement of Mechanical Properties and Fatigue Testing

Quasi-static Tensile

The quasi-static properties of the composite material were obtained for each batch of pre-conditioned specimens. A screw driven Instron tensile testing machine was used to measure the quasi-static tensile strength and stiffness. Strain data was recorded with an extensometer, and transverse and axial strains were obtained using CEA-13-125WT-350[1] strain gages. Gages were attached to the wet specimens using a cynoacrylate adhesive (M-bond 200)[1]. Specimens were tested at a displacement rate of 2.5 mm/min.

Fatigue Testing

Fatigue experiments were conducted under the following loading and environmental conditions:

1)   Loading mode: tension/tension

2)   R (minimum stress to maximum stress ratio) = 0.1

3)   Loading level (S_{max}): 30 %, 35 %, 40 %, and 45 % of ultimate tensile strength (UTS)

4)   Test frequency: 2 Hz and 10 Hz

5)   Exposure environment: air, filtered tap water, and 3.5 % mass fraction NaCl in distilled water (simulated sea water).

6)   Test temperature: 4 $^{\circ}$C, 30 $^{\circ}$C and 65 $^{\circ}$C.

All fatigue specimens were tested using a 4.5 x 10^4 N MTS servo-hydraulic machine; a schematic sketch of the experimental setup is displayed in Figure 5a, and a corresponding photograph is shown in Figure 5b. The fluid cell (with the specimen enclosed) was connected to the solution circulation bath using polyurethane tubing. A thermometer attached to the cell provided a means to continuously monitor the temperature of the solution in the cell. After the appropriate stress levels were entered into the data acquisition system and the desired frequency (fatigue) was selected, the circulating system was turned on. This same procedure was employed for fatigue testing at 2 Hz and 10 Hz frequencies. S-N curves were generated for the composite

13

material by cycling the coupons to failure and recording the number of cycles-to-failure. The residual mechanical properties of the material were measured after fatiguing the specimens to a preset number of cycles. The tensile modulus and Poisson's ratio of these specimens were then determined using a screw-driven Instron testing machine.
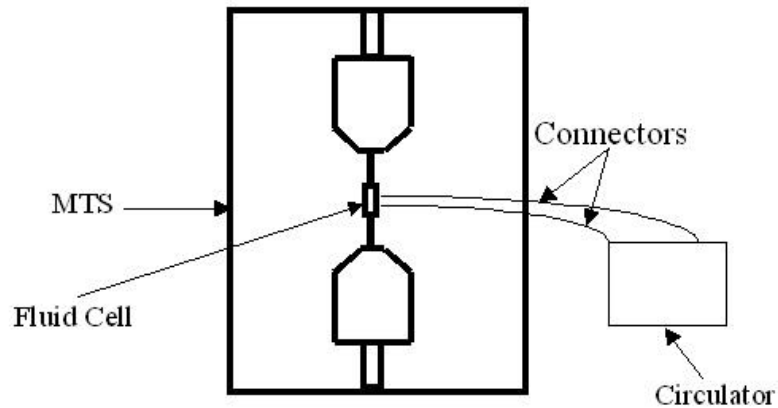

Figure 5a: A schematic of the experimental setup to measure fatigue life of polymer composite in simulated seawater at a desired temperature.
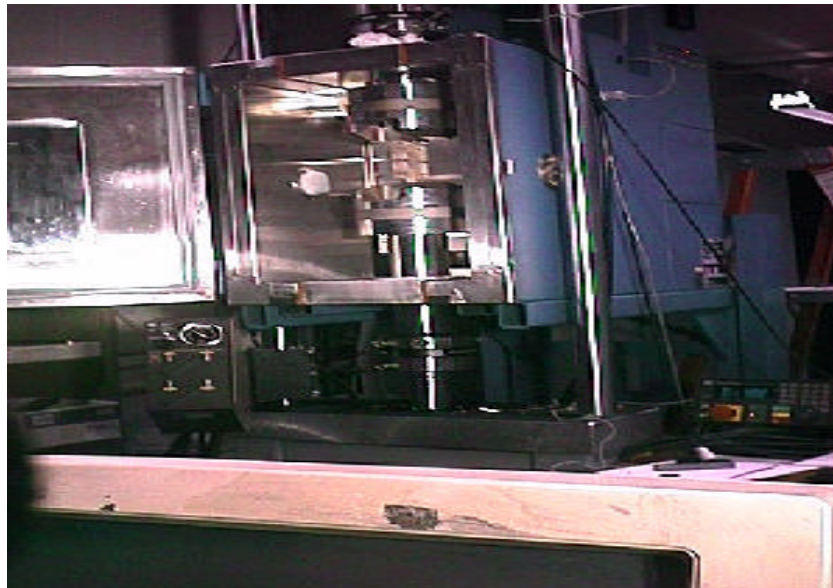

Figure 5b: Photograph of the experimental setup to measure fatigue life of polymer composite in simulated sea water at a specified temperature.

Test Matrix for Fatigue

Table 1 presents the test matrix used to study the fatigue life of E-glass fiber/vinyl ester composites under different loading conditions at each temperature in each environment, i.e., ambient air, fresh water, or simulated sea water. Each batch of the saturated specimens was allocated to a particular set of tests. For instance, the batch of specimens used to generate S-N curve at 10 Hz was also employed to measure the residual mechanical properties at 10 Hz as well. The numbers noted in Table 1 at a given stress level and load cycles represent the number of replicates. For example, at 2 Hz, 35 % UTS load level and 10^4 cycles, three specimens were usually tested.

Table 1: Test matrix showing number of replicates performed for fatigue test of polymer composite under different loading conditions

Load levels (S_{max})	2 Hz Preset Cycles			10 Hz Preset Cycles							
	10^3	10^4	10^5	10^3	10^4	10^5	2×10^5	5×10^5	10^6	2.5×10^6	5×10^6
30 %	0	0	0	0	0	0	0	1	2	1	1
35 %	3	3	3	5	5	6	0	0	4	0	0
40 %	3	3	3	5	5	6	3	0	0	0	0
45 %	3	3	3	8	6	6	0	0	0	0	0

RESULTS AND DISCUSSION

Uptake of Salt Solution in Composite

As indicated earlier, all specimens were fully saturated with water or simulated sea water prior to fatigue testing. Further, to speed up the sorption process, the solution was heated at 65 °C. Figure 6 presents the sorption behavior of the simulated seawater in the composite as a function of time at 65 °C. Each experimental data point is the average of seven specimens. After approximately 450 h, the simulated sea water nearly saturates the composite, reaching 0.9 % equilibrium mass fraction. This immersion time was used for pre-saturating all remaining specimens before fatigue cycling. The dashed line in Figure 6 represents a theoretical prediction using a Fickian model described in Reference 20.
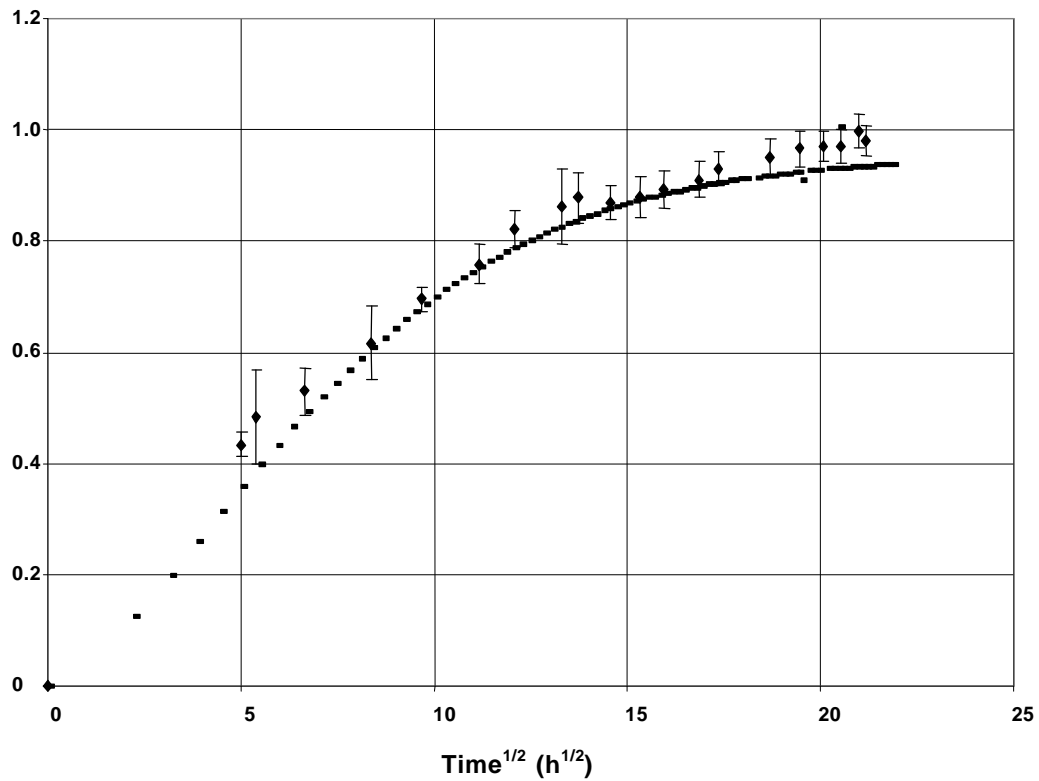
Figure 6: Sorption behavior of simulated sea water at 65 ^{o}C in the test composite (♦ experimental values, ■ Fickian prediction). Error bars represent one standard deviation.

16

The experimental data of Figure 6 were used to calculate the diffusion coefficient of composite in simulated seawater solution using the following expression (20):

$$D_z = p \frac{h}{16M_m^2} \left(\frac{M_2 - M_1}{\sqrt{t_2} - \sqrt{t_1}} \right)$$

(28)

where:

D_z: the diffusion coefficient

h : thickness of composite

M_1, M_2 : two levels of mass uptake in the linear region

t_1, t_2 : times in the linear region corresponding to M_1 and M_2.

D_z of the vinyl ester/E-glass fiber composite used in this study was approximately 2.9 x 10^{-8} cm^2/s in simulated sea water at 65 °C. A similar value was recorded for specimens immersed in fresh water at 65 °C, suggesting that water was the main component sorbed in the composite. The diffusion coefficients for a vinyl ester resin commonly used for polymer/fiber composites in water at 30 °C and 60 °C have been reported to be 0.9 x 10^{-8} cm^2/s and 2.4 x 10^{-8} cm^2/s, respectively (21).

Mechanical Properties

Before Exposure and After Saturation with Fresh Water and Simulated Sea Water

Mechanical properties of the composite were measured before exposure (as received) and following saturation with fresh water and simulated sea water at 65 °C. As indicated earlier, eleven specimens were tested in the as-received condition and seven specimens were tested after exposure. Table 2 provides the tensile strengths, tensile moduli, and Poisson's ratios and their corresponding standard deviations for the composite exposed to three environments. Decreases of 25 % and 32 % in the tensile strength are observed for samples saturated with fresh water and simulated seawater at 65 °C, respectively. Further, saturation in water and the same salt solution also resulted in a reduction in the tensile modulus of 15 % and 11 %, respectively. The differences between samples tested before exposure and after water and simulated sea water saturation were statistically significant at 95 % confidence level, as determined by the t-test analysis. However, no significant difference was observed between the water-saturated and

17

simulated sea water-saturated specimens for the same mechanical properties. On the other hand, the Poisson's ratio was essentially unchanged for both fresh water and simulated sea water exposure.

Table 2: Mechanical properties of E-glass/vinyl ester composite before exposure and after saturation with fresh water and simulated sea water

	Dry		Fresh Water		Simulated Sea Water	
	Mean	Std dev	Mean	std dev	Mean	std dev
Ultimate tensile strength (MPa)	212	17.9	158	13.4	144	14.4
Modulus (GPa)	15.55	0.66	13.28	1.20	13.85	4.01
Poisson's Ratio	0.31	0.03	0.31	0.03	0.33	0.04

Fatigue Experiments

As indicated in the experimental section, the effects of ultimate tensile stress, cyclic frequency, cyclic temperature, and exposure environments on the fatigue behavior of the composite were investigated to provide inputs for the fatigue model. The fatigue experiments were conducted at four different levels of ultimate tensile stress (UTS) and at two frequencies in air, fresh water and simulated seawater and at three different temperatures (4 ^{o}C, 30 ^{o}C, and 65 ^{o}C). Some representative data on the effects of these parameters on fatigue properties are presented in this section. However, discussions of these results are treated in the model verification section.

The effects of cycling frequency, exposure environments, and the temperature at which fatigue experiments were conducted are illustrated in Figures 7, 8 and 9, respectively. In these figures, the normalized % UTS (with respect to the value of the as-received material) is plotted against the number of cycles at failure. Except for fatigue testing in air, all specimens were completely saturated with their respective solutions (18 days immersed in solution) before testing. Further, all failures were observed to occur within the fluid cell.

Figure 7 is a S-N plot for specimens fatigued at 2 Hz and 10 Hz in simulated sea water at 30 °C. A slightly steeper slope for specimens tested at 2 Hz is observed compared to those at 10 Hz, suggesting that the deterioration of the composite was greater at 2 Hz than at 10 Hz.
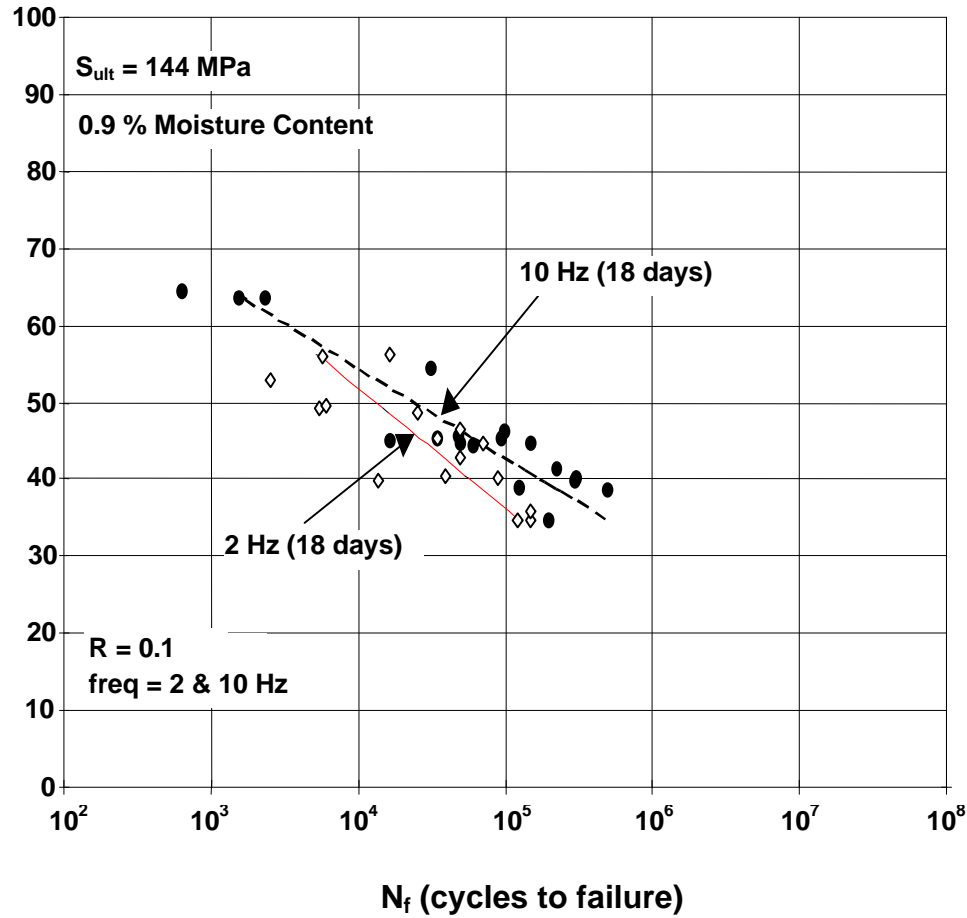

Figure 7: S-N plot of a vinyl ester/glass composite fatigued at 2 Hz (◊) and 10 Hz (●) in simulated sea water at 30 °C.

The influence of the exposure environment on fatigue behavior of the composite is displayed in Figure 8. These S-N plots were generated for specimens cycled at 10 Hz in air, fresh water, and simulated sea water at 30 °C. Although the exposure environment appears to have little effect on the slope of the curves, the presence of aqueous solutions caused a substantial decrease on the total life time. Figure 8 indicates that subjecting this composite material to a fresh water or simulated sea water at 30 °C can result in a reduction of approximately one decade of its fatigue life as compared to that in air under the same loading condition.
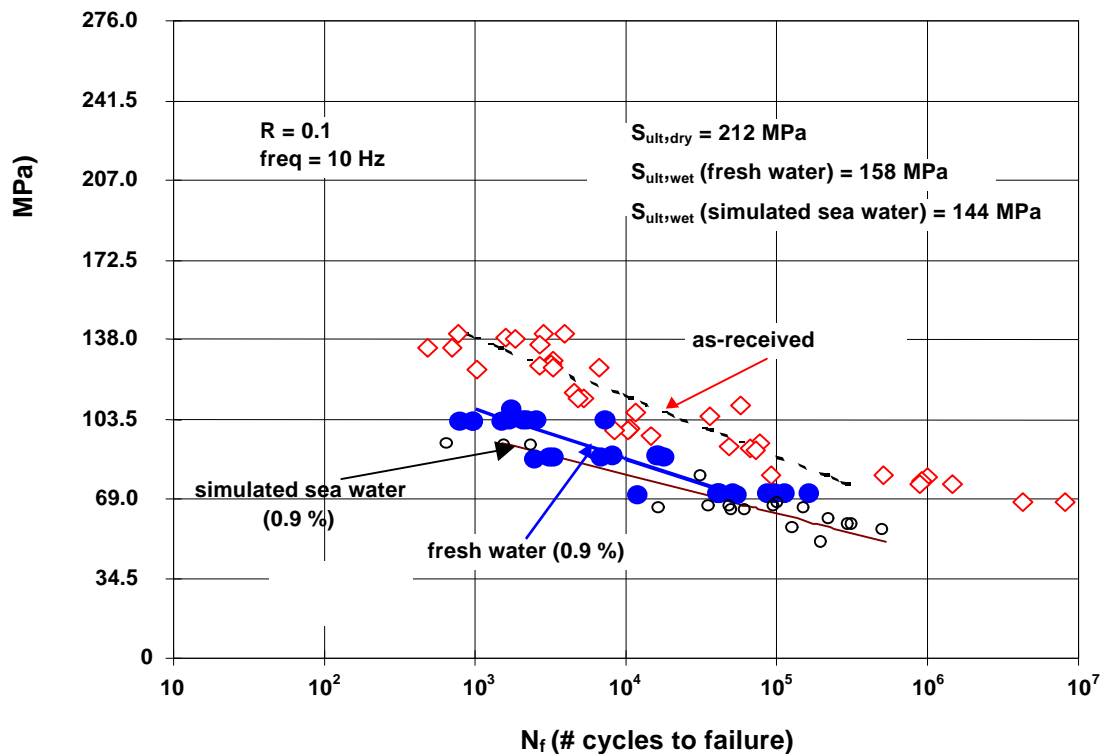
19

Figure 8: S-N plot of a vinyl ester/glass fiber composite fatigued at 10 Hz in air( ), fresh water($\bullet$), and simulated sea water (o) at 30 ^{o}C.

Figure 9 displays the S-N data for the composite cycling at 10 Hz in simulated sea water at three different temperatures (4 ^{o}C, 30 ^{o}C and 65 ^{o}C). These temperatures represent a wide range of environments to which the polymer composites for civil engineering applications may be subjected. The results show that the losses in both the amplitude and rate of fatigue were smaller at 4 ^{o}C than at 30 ^{o}C or 65 ^{o}C. Except for low cycles (10^3) where little difference exists between the two temperatures, the reduction at 65 ^{o}C appears to be greater than that at 30 ^{o}C. Since the difference between 65 ^{o}C and 30 ^{o}C is relatively small, additional data is required to provide a more definite conclusion.
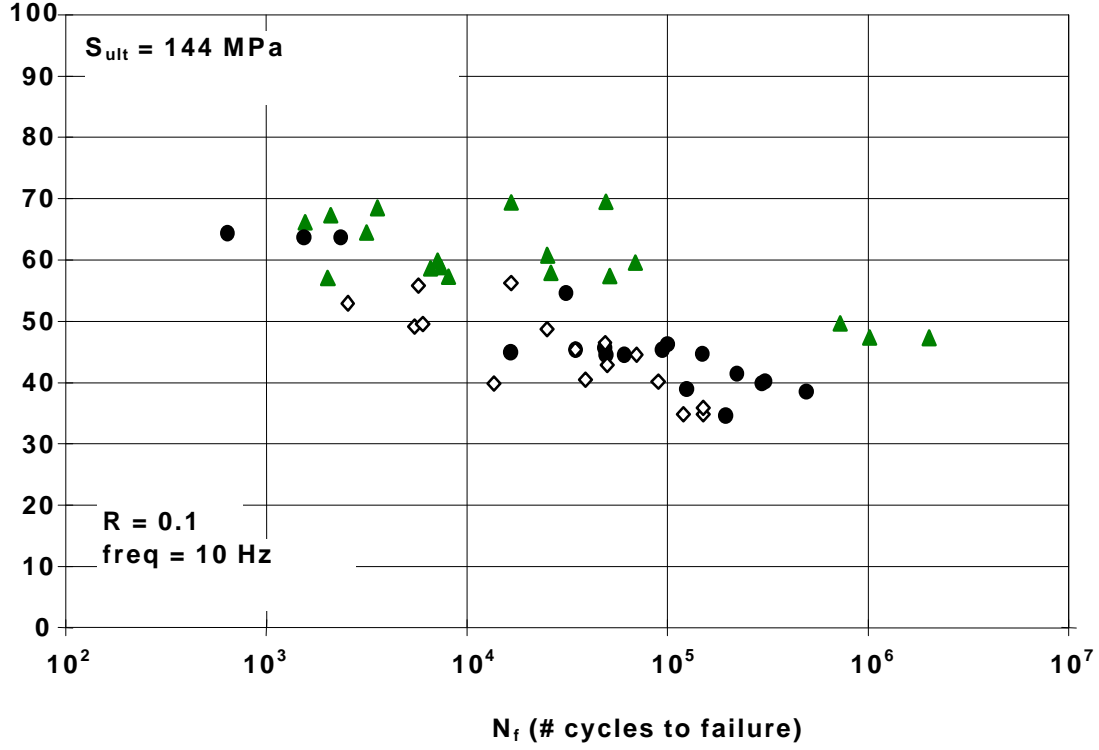
Figure 9: S-N plot of a glass fiber/vinyl ester composite fatigued at 10 Hz in simulated sea water at 4 °C (▲), 30 °C (●), and 65 °C(   ).
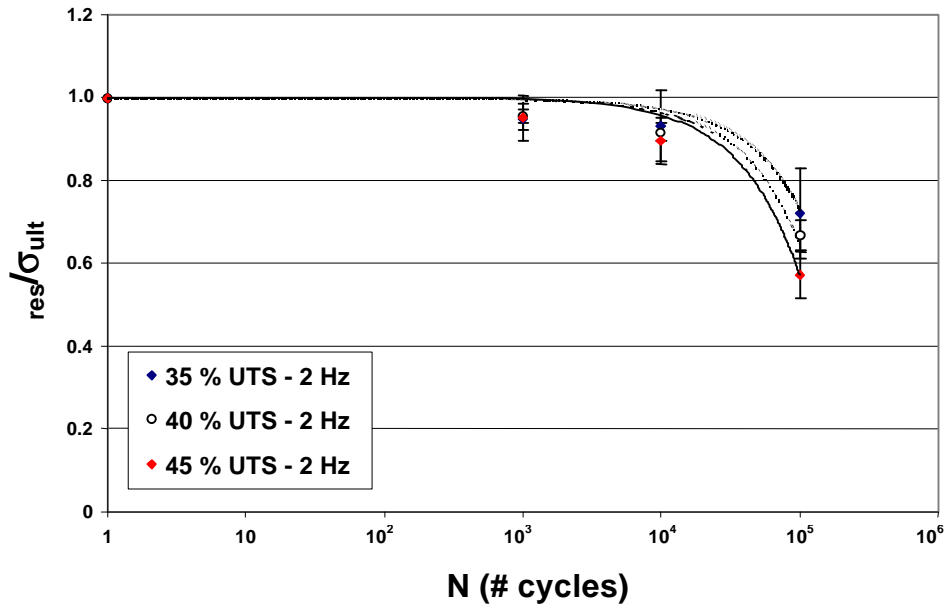
Residual Strength and Modulus

The residual strengths and moduli of composites fatigued at specified cycles were recorded for different loadings and frequencies in simulated sea water at 30 °C. The data were fitted to the following equation (Eq. 29) given by Broutman-Sahu [22] with an $\alpha = 1$.

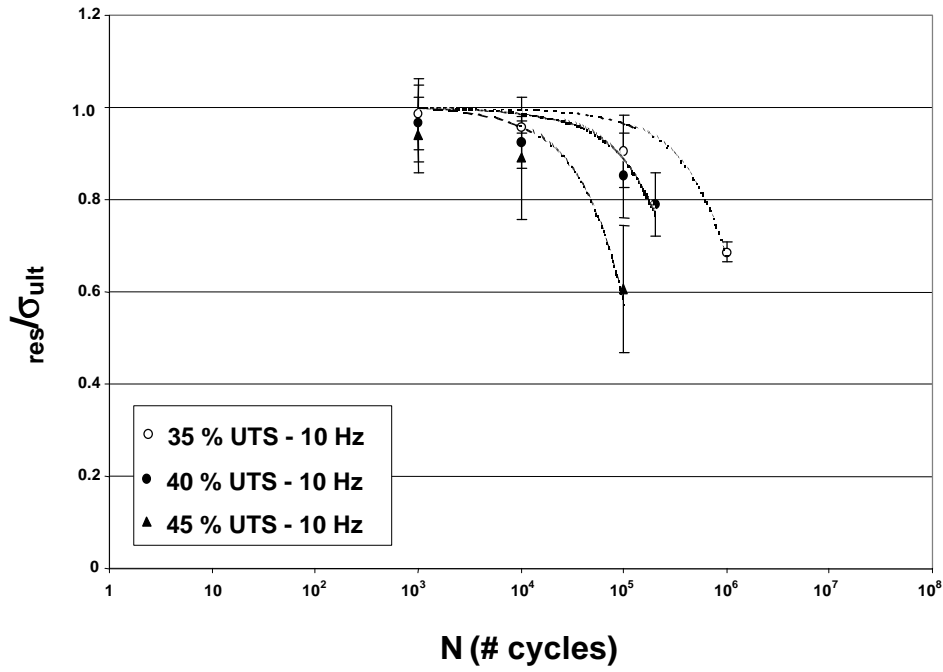$$\frac{S_{res}}{S_{ult}} = 1 - \left(1 - \frac{S_a}{S_{ult}}\right)\frac{\text{constant}}{N^a} \tag{29}$$

where σ_{res} is the residual tensile strength, σ_{ult} is the the ultimate tensile strength, σ_a is the applied stress, and N is the number of cycles. Figures 10a and 10b give the residual strength plots for loading levels at 2 Hz and 10 Hz, respectively, showing progressive damage with increased loading levels at either frequency.

21

The effects of frequency on the residual strengths at a particular loading stress are presented in Figure 11, in which the results for 35 % UTS and 40 % UTS are shown. Plots of residual strengths vs number of cycles at other loading levels are similar to that of Figure 11. In general, the reduction in strength at 2 Hz is slightly greater than that at 10 Hz, similar to that observed for the S-N behavior.

The residual modulus characterizes changes in the stiffness of the composite when subjected to preset cyclic loading. The residual moduli for several loading levels at 2 Hz and 10 Hz in simulated sea water are shown in Figure 12a and 12b, respectively (the lines in these figures are the fitted curves). From these results, the change in stiffness (damage) appears to be more prominent at 40 % UTS and 45 % UTS than at 35 % UTS, indicating that the applied load has an influence on the residual modulus of the glass fiber/vinyl ester composite.
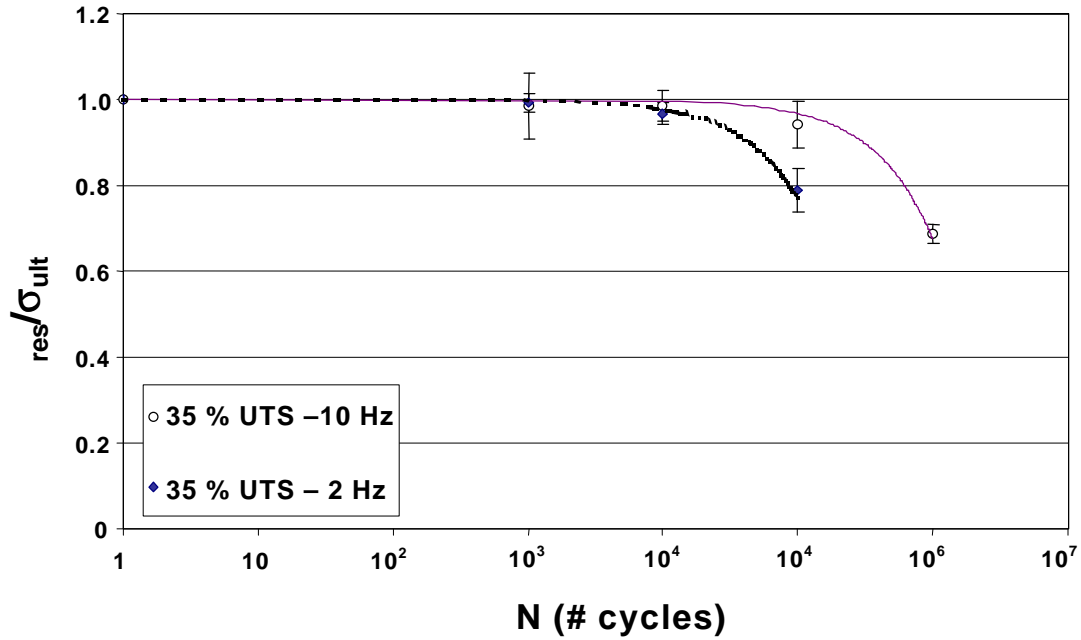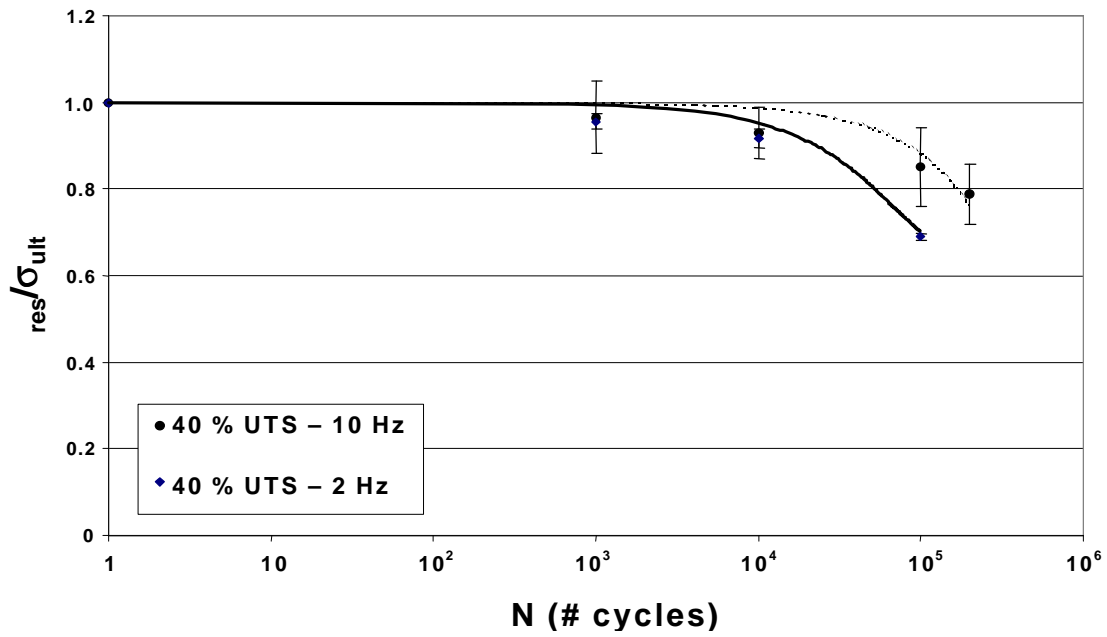
(a)

(b)

Figure 10: Residual strength as a function of loading cycles N for several load levels at (a) 2 Hz and (b) 10 Hz in simulated sea water at 30 $^{\circ}$C (error bar represents one standard deviation).

(a)

(b)

Figure 11: Effects of cyclic frequency on residual strength of test composite fatigued at several loading conditions: (a) 35 % UTS and (b) 40 % UTS in simulated sea water at 30 $^{\circ}$C (error bar represents one standard deviation).
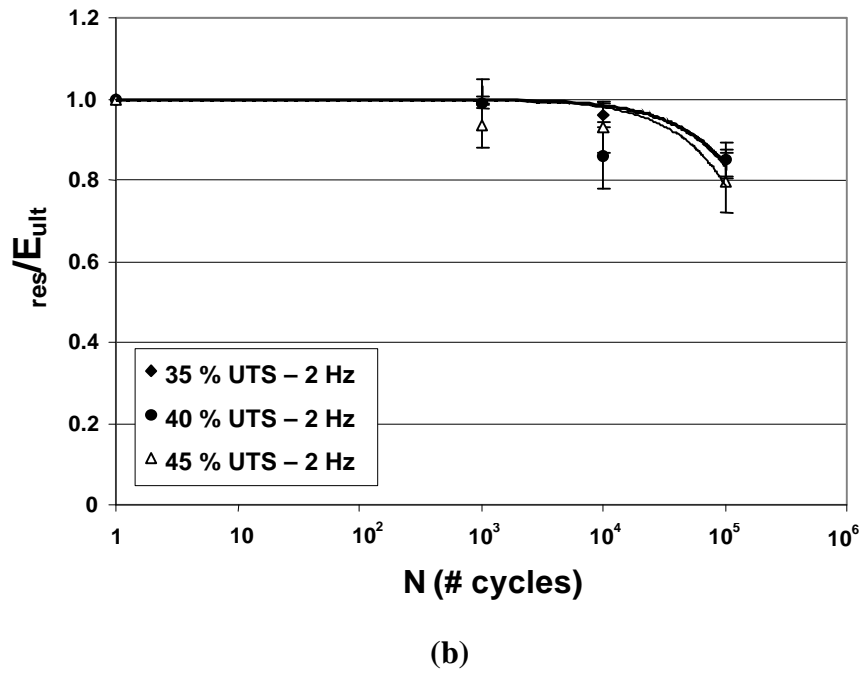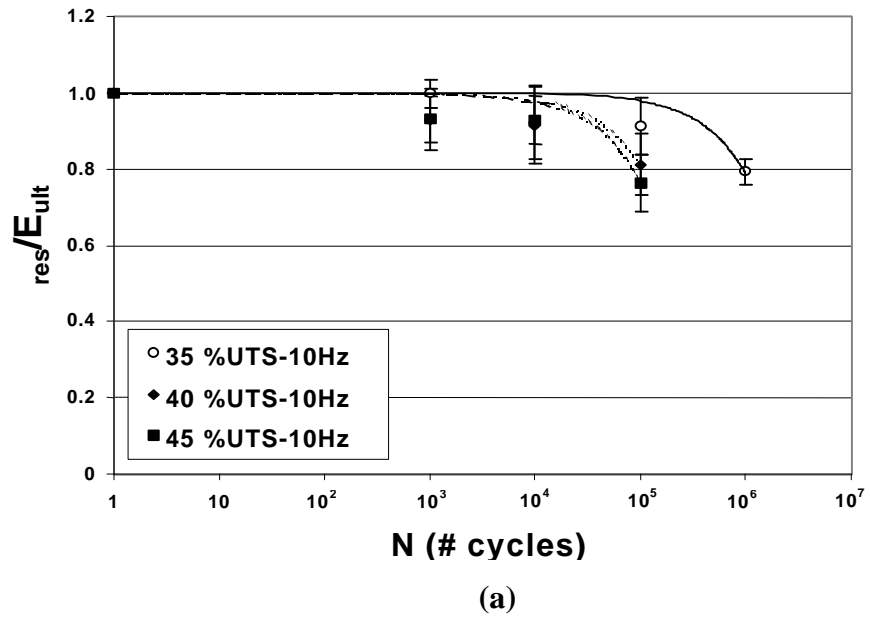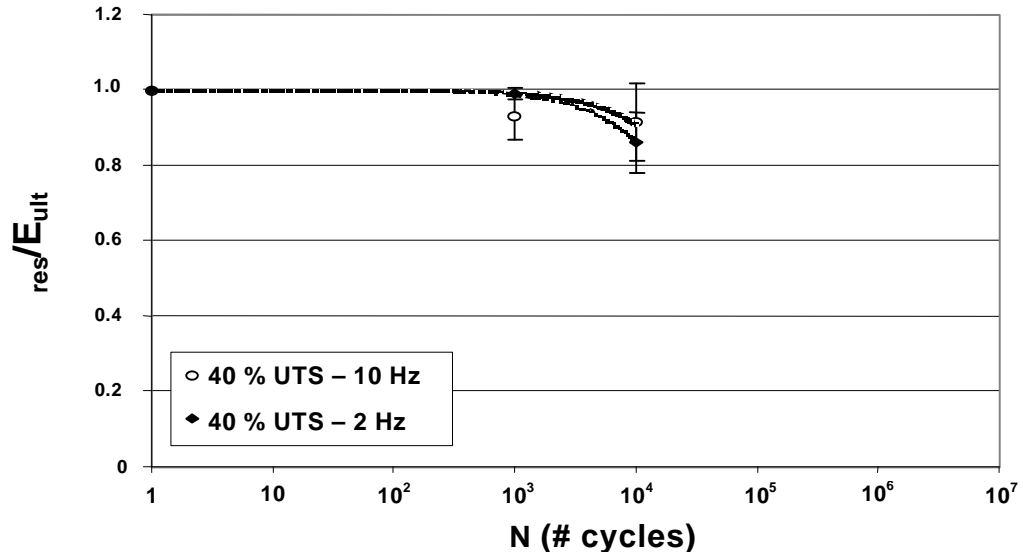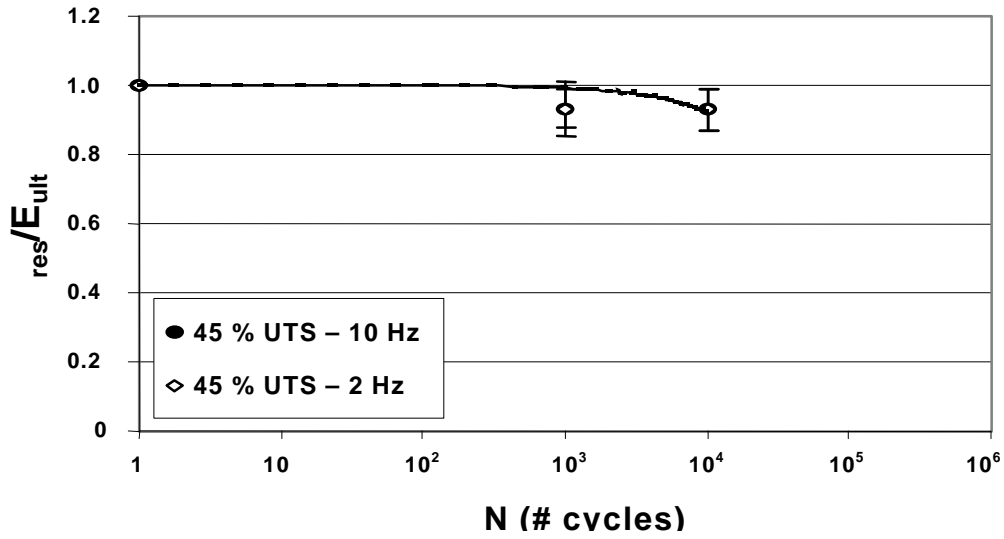
Figure 12: Residual modulus as a function of loading cycles for three load levels for 2 Hz (a) and 10 Hz (b) in simulated sea water at 30 $^{\circ}$C (error bar represents one standard deviation).

Comparative plots of residual modulus for test frequencies of 2 Hz and 10 Hz at a particular loading level are displayed in Figures 13a and 13b, respectively, for two loading levels. In these plots, the error bars overlap considerably, suggesting a negligible difference in modulus reduction between 2 Hz and 10 Hz experiments.

(a)

(b)

Figure 13: Effect of cyclic frequency on residual modulus at a particular loading level for (a) 40 %UTS and (b) 45 % UTS in simulated sea water at 30 $^{\circ}$C (error bar represents one standard deviation).

Residual Poisson's Ratio

        The Poisson's ratios were obtained at 2 Hz and 10 Hz in simulated sea water at 30 $^{\circ}$C. Normalized plots (with respect to as-received value) are presented in Figures 14a and 14b. No significant changes in the residual Poisson's ratio with number of cycles were observed. The fairly even distribution of data on Poisson's ratio may be attributed to the higher proportion of unidirectional fiber in the crosswise direction, resulting in a strong resistance to change in the transverse direction.

(a)   (b)

Figure 14: Residual Poisson's ratio as a function of cycles N for several loading levels at (a) 2 Hz and (b)10 Hz in simulated sea water at 30 $^{\circ}$C.

MODEL VERIFICATION

        Figure 15 displays the predicted S-N curves and experimental fatigue data for the vinyl ester composite tested in air, fresh water, and simulated sea water at 30 °C. In this figure, the maximum stress is plotted against the number of cycles at failure on a log-log scale. Values of the square of correlation coefficient (r^2) between the experimental maximum stress and the

number of cycles at failure are 0.856 for ambient air, 0.803 for fresh water, and 0.840 for simulated seawater. The same fatigue data are also plotted in semilog scale (i.e., $\sigma_{max} = m \log N_f + C$, Equation 18); this result is shown in Figure 16. In this case, the r^2 value for dry air, fresh water, and simulated seawater environments are 0.824, 0.794, and 0.863, respectively. The square of the linear correlation coefficient quantitatively indicates the linear correspondence between two variables [23], e.g., maximum stress and the number of cycles at failure in this case. An r^2 value of 1.0 means a perfect linear relationship between the two quantities; a value less than 1.0 means a less good fit. Based on these r^2 values, both formulas (Equations 8 and 18) can be used to predict fatigue life of the polymer composite used in this study. However, combining with additional tests at lower load levels that failed at a higher number of cycles, Eq. 8 gives a higher r^2 value than Equation 18. Therefore, Equation 8 is better suited to describe the fatigue with a wider range of life time.

In Figure 15, little difference in the slopes of the regression lines for ambient air, fresh water, and simulated seawater is observed, suggesting that the same mechanism of failure may be operative in all three environments. The slopes of the regression lines are in the range (10 % to 11 %) UTS per decade, which are consistent with earlier results [24]. Also, although the difference in fatigue behavior between fresh water and simulated sea water is small, the fatigue life of the composite in fresh water or simulated salt water is shorter than that in ambient air. Thus, the presence of water alone has a significant effect on the durability of this material; this result is in agreement with previous observations [24,25]. The loss of fatigue life of polymer composites has been explained by the stress corrosion mechanism [26]. Based on this concept, the strength of E-glass fiber is controlled by the chemical reaction of the glass with the surface-sorbed water. This reaction removes certain chemical elements from the fiber, resulting in microflaws (stress concentration locations), which are the precursors to fiber fracture. This process is irreversible. Thus, it appears that the stress concentration developed along the fiber surface does not change the mechanism of fatigue failure, but rather, reduces the ultimate strength.
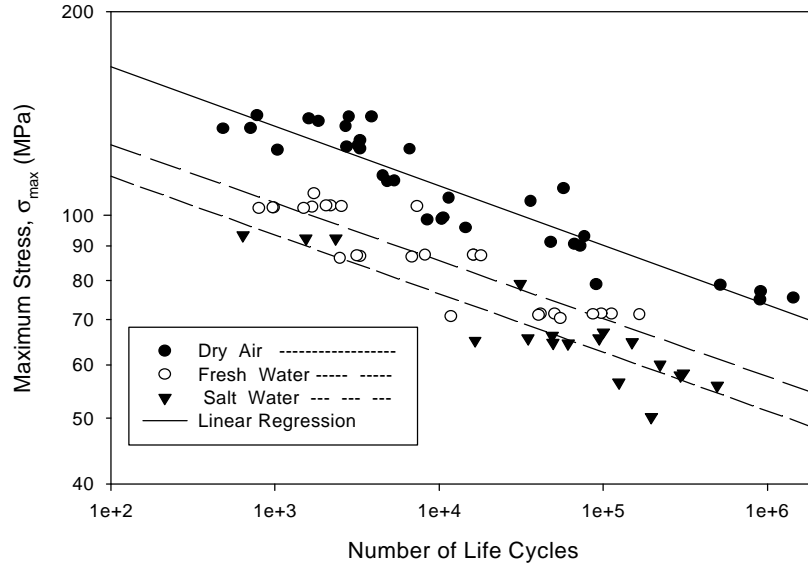
Figure 15: Predicted S-N curves and experimental fatigue data in log-log scale of the test composite fatigued in air, fresh water, and simulated seawater at 30 $^{\circ}$C.

Figure 16: Predicted S-N curves and experimental fatigue data in semi-log scale of the test composite fatigued in air, fresh water, and simulated seawater at 30 $^{\circ}$C.

Figure 17 shows the normalized predicted S-N curves and normalized experimental S-N data of the composites fatigued in air, fresh water and simulated sea water. The normalized values were obtained by dividing the maximum applied stress by its respective ultimate strength

at a particular exposure and loading condition. The closeness of the regression curves in this figure suggests that a single normalized S-N curve can be used to predict the fatigue life of a vinyl ester/E-glass fiber composite exposed to all three environments. The good fit between the experimental data and Equation 8, as shown in Figure 15, suggests that the model is valid for predicting the fatigue life of the polymer composites used in this study under a wide range of loading and exposure conditions.

Figure 17: Predicted normalized S-N curves and experimental fatigue data for the test composite in air, water, and simulated seawater at 30 $^{\circ}$C.

In order to determine the value of the material constant m, Eq. 19 is rewritten into a simple linear form (y=a+bx):

$$\log(S_{max}) = -\frac{1}{2m}\log\left[(n+1)(C(1-R)^{m})\right] - \frac{1}{2m}\log N_{f}$$

$$= \frac{1}{2m}\log\frac{1}{(n+1)(C(1-R)^{m})} - \frac{1}{2m}\log N_{f} \qquad (30)$$

such that

$$a = \frac{1}{2m}\log\frac{1}{(n+1)(C(1-R)^{m})} \qquad (31)$$

30

$$b = -\frac{1}{2m} \tag{32}$$

Values of a and b are obtained from separate fatigue experimental data at 10 Hz in dry air, fresh water and salt water environments; and m can be obtained from -1/2b. Table 3 presents these values and their standard errors for the three environments.

Table 3: The linear constants and m values for three environments

	a	Std. Error	b	Std. Error	m	Std. Error
Dry Air	0.0701	0.0272	-0.0882	0.0065	5.67	0.42
Fresh Water	0.0766	0.0340	-0.0859	0.0085	5.82	0.53
Salt Water	0.0729	0.0450	-0.0869	0.0095	5.75	0.64
Combined	0.0756	0.0181	-0.0877	0.0042	5.70	0.23

The small differences among the a and b values in the three environments confirms that a single normalized S-N curve can be used to predict the fatigue life in three environments.
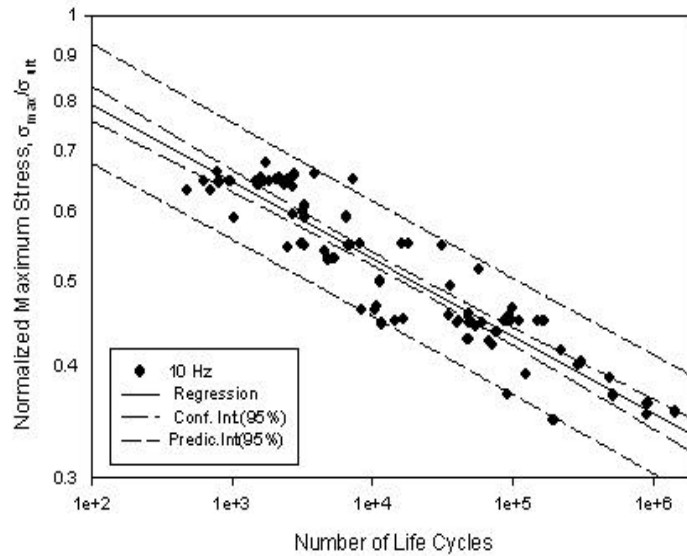

Figure 18: Predicted normalized S-N curves and experimental fatigue data for the test composite in all three environments.

31

Figure 18 depicts the single linear regression that combines all experimental fatigue data of the three environments. The 95 % confidence interval and the 95 % prediction interval are also shown. Overlaying the plots in Figure 17 and Figure 18, the three S-N curves for three environments lie well within the 95 % confidence interval. Thus, the error induced by a single normalized S-N curve is well within the measurement uncertainty. Therefore, a single S-N curve (described by Eq. 33) can be used to predict the fatigue life of a E-glass fiber/vinyl ester composite exposed to air, fresh water, or simulated seawater. The corresponding combined values of a, b, m, and their standard errors are presented in Table 3.

When a and b values are substituted into Eq. 17, the S-N curve for a E-glass/vinyl ester composite at 10 Hz and $N_f \geq 10$ may be expressed as:

$$(S_{max})^{11.40}N_f = 7.28 \quad \textit{for the three environments combined together} \quad (33)$$
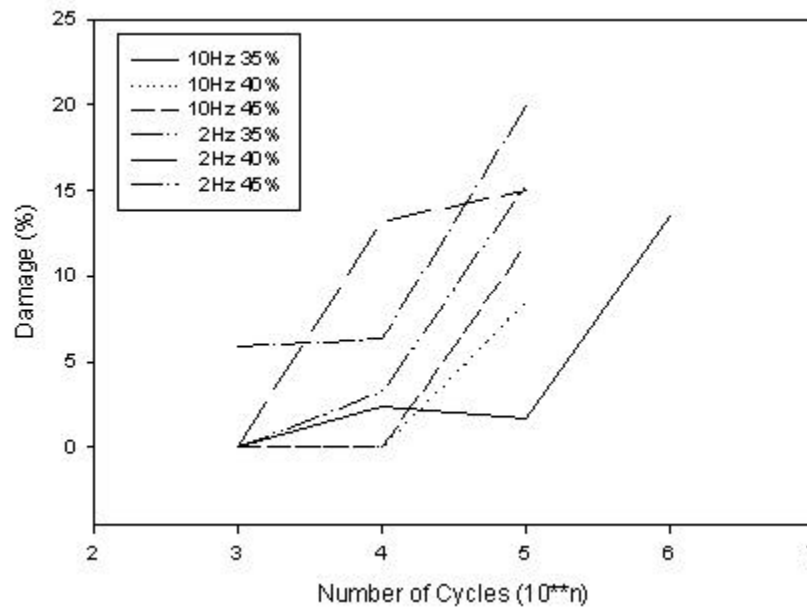

Figure 19: Partial damage at selected loading cycles for 2 Hz and 10 Hz.

The value of n may be determined from the partial damage data at different numbers of loading cycles under a given maximum load, which are given in Figure 19 for 2 Hz and 10 Hz. It is interesting to note that whenever severe damage has occurred, the lines become parallel. In other words, when the damage becomes substantial, it increases at a constant rate. Since we only measured the partial damage at the beginning of each order of magnitude, i.e., 10^3, 10^4, 10^5, and 10^6 cycles, we may not accurately record the number of cycles where the substantial damage starts. Figure 19 suggests that the damage growth within an order of magnitude (dD/dlog N) is constant and equals approximately 0.12. Therefore, for a given maximum applied load with two partial damages D_1 and D_2 measured at two respective numbers of loading cycles N_1 and N_2, we have:

$$\frac{N_2}{N_1} = 10 \tag{34}$$

and

$$\frac{dD}{d \log N} = \frac{D_2 - D_1}{\log(N_2) - Log(N_1)} = \frac{D_2 - D_1}{\log \frac{N_2}{N_1}} = D_2 - D_1 = 0.12 \tag{35}$$

From Figure 19, D_1 starts from approximately 1 % to 5 % . Therefore,

$$\frac{D_2}{D_1} = \frac{D_1 + 0.12}{D_1} = 1 + \frac{0.12}{D_1} = 1 + (2.4 \ to \ 12) \tag{36}$$

Consequently, from Eq. 25, we may have:

$$K_{12} = \frac{N_1}{N_2} \frac{D_2}{D_1} = 0.34 \ to \ 1.3 \tag{37}$$

However, from Eq. 6 and Figure 4, n must be ≥ 1:

$$n = \frac{2(1 - K_{12})}{(D_1 - D_2 K_{12})} \geq 1 \tag{38}$$

$$K_{12} \geq \frac{2 - D_1}{2 - D_2} = \frac{2 - D_1}{2 - 0.12 - D_1} \approx 1.065 \tag{39}$$

$$1.065 \leq K_{12} \leq 1.3 \tag{40}$$

$$n = \frac{2(1 - K_{12})}{(D_1 - D_2 K_{12})} \approx \frac{2(K_{12} - 1)}{K_{12}(D_2 - D_1)} \tag{41}$$

Thus we have:

$$1.02 \leq n \leq 3.85$$

More experiments are required to determine the value of n. However, based on our limited experimental data, the n value should be closer to the lower bound. For now, we set n equal to 2.

To determine the C parameter, experimental data at two frequencies are used. Figure 20 displays the linear-fit S-N lines for the simulated seawater environment at 2 Hz and 10 Hz frequencies. From this figure, it appears that for a given maximum applied load, the number of cycles at failure for 2 Hz is less than that for 10 Hz. It is also evident that, at lower cycles-to-failure, the two plots appear to converge. The effect of cyclic frequency on the fatigue behavior of polymer composites has been reported (27-30), for which the residual modulus and residual strength of specimens that had been cycled at lower frequency were lower than those fatigued at higher frequency.
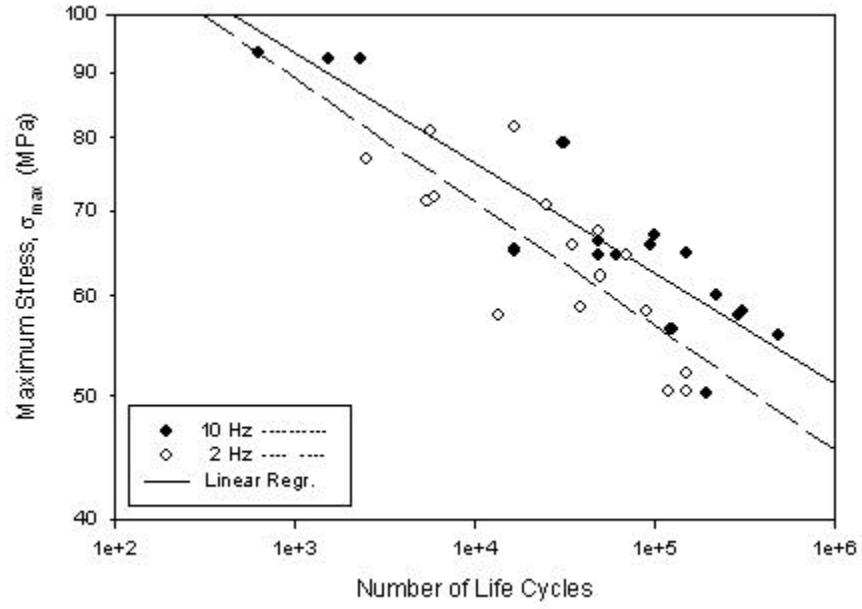
34

Figure 20: Predicted S-N curves and experimental fatigue data for the test composite at 2 Hz and 10 Hz in simulated sea water at 30 $^{\circ}$C.

The small difference between the slopes of the S-N curves for 2 Hz and 10 Hz in Figure 20 could be due to an inability to statistically average out experimental variations by the limited number of samples. The scattering of the experimental data from the S-N curve for 2 Hz is obviously greater than that for 10 Hz. If we reconstruct the S-N curve for 2 Hz using the same slope of the S-N curve for 10 Hz as shown in the dot line, the newly constructed S-N curve reasonably fits the experimental data for 2 Hz. From this analysis, we can conclude that the slope of S-N curve is not sensitive to frequency, and neither is the m value.

The parallel partial damage curves in Figure 19 for 2 Hz and 10 Hz indicates that, for the composite used in this study, n is not sensitive to frequency. Any sensitivity to frequency must lie in the C constant. If we assume that composites fatigued at a lower frequency fail at a lower number of cycles for a given maximum applied load, then the C constant will be higher at a lower frequency, i.e.:

$$C = C_1 + \frac{C_2}{f} \tag{42}$$

where C_1 and C_2 are constants and f is the frequency. Substituting $\mathbf{C}$ into Eqs. 14 and 15, we obtain:

$$\frac{1}{n+1} - \frac{(1-D)^{n+1}}{n+1} = (C_1 + \frac{C_2}{f})(S^2_{max}(1-R))^m N_f \tag{43}$$

$$\frac{1}{n+1} = (C_1 + \frac{C_2}{f})(S^2_{max}(1-R))^m N_f \tag{44}$$

By taking a logarithm of both sides of Eq. 44 and substituting σ_{max} and N_f for 2 Hz and 10 Hz, respectively, into the equation, two separate equations for 2 Hz and 10 Hz can then be subtracted from each other. These two parallel S-N curves relate C_2/f to C_1, as expressed in Equations 45 through 47:

$$\log(C_1 + \frac{C_2}{2}) - \log(C_1 + \frac{C_2}{10}) = 2m(\log S_{max,10} - \log S_{max,2}) = 0.445 \tag{45}$$

where $\sigma_{max,10}$ and $\sigma_{max,2}$ are the maximum stresses for 10 Hz and 2 Hz, respectively.

$$\frac{C_1 + \frac{C_2}{2}}{C_1 + \frac{C_2}{10}} = 2.78 \tag{46}$$

$$\frac{C_2}{C_1} = 8 \tag{47}$$

Eq. 43 and Eq. 44 can then be rewritten as:

$$\frac{1}{n+1} - \frac{(1-D)^{n+1}}{n+1} = (C_1 + \frac{8}{f})(S^2_{max}(1-R))^m N_f \tag{48}$$

$$\frac{1}{n+1} = (C_1 + \frac{8}{f})(S^2_{max}(1-R))^m N_f \tag{49}$$

36

As for partial damage, Figure 19 shows that the residual modulus is higher at 10 Hz than at 2 Hz, which is consistent with previous studies cited earlier.

SUMMARY AND CONCLUSIONS

A fatigue model based on the cumulative damage due to cyclic loading is developed and verified with experimental data for a glass fiber/vinyl ester composite. The fatigue damage per cycle, residual modulus in terms of partial damage, and fatigue life of fiber-reinforced polymeric composites are described as functions of applied stress, stress amplitude, loading frequency, state of damage, and materials constants as follows:

$$\frac{dD}{dN} = (C_1 + \frac{C_2}{f}) \frac{(S^2_{\max}(1-R))^m}{(1-D)^n}$$

$$\frac{1}{n+1} - \frac{(1-D)^{n+1}}{n+1} = (C_1 + \frac{C_2}{f})(S^2_{\max}(1-R))^m N$$

$$\frac{1}{n+1} = (C_1 + \frac{C_2}{f})(S^2_{\max}(1-R))^m N$$

The material constants used in the model are determined using the experimental data. This model can be used to predict the fatigue life of an E-glass/vinyl ester polymer composite at an applied load and to predict the residual strength modulus after a number of cycles at a given load in various civil engineering and offshore environments. Using the experimental data to determine the model constants, we have obtained the following S-N curve for a glass fiber reinforced vinyl ester composite exposed to the three environments:

$$S_{\max}^{11.40} N_f = \frac{13.11}{1 + \dfrac{8}{f}}$$
$\qquad$ *for the three environments combined*

where $S_{\max}$ is the normalized stress to respective static ultimate strength ($\left| S_{\max} \right| \leq 1$).

The residual modulus for a given maximum applied load after **N** loading cycles can be predicted as:

$$\frac{E}{E_o} = \left(1 - \frac{S_{\max}^{11.40} N \left(1 + \dfrac{8}{f} \right)}{13.11} \right)^{\frac{1}{n+1}}$$
$\qquad$ *for the three environments combined*

The value of n is not conclusive at this time, and more experiments are required to determine its value.

The damage tolerance and durability of E-glass/vinyl ester composite is adversely affected by exposure to the simulated saltwater environment. The presence of the moisture alone enhances the damage. A drop of about 11 % in modulus and 32 % in strength, respectively, was observed for specimens pre-conditioned in fresh water and simulated sea water at 65 °C and tested quasi-statically. Stress corrosion is suspect in the degradation of this composite system. Initial strength loss observed under various conditions namely: salt, dry and water, exhibit a similar trend indicating that failure mechanisms are similar and dominated by fiber damage process. Normalized fatigue stress against percent ultimate tensile strength indicates a slope of about 10 % UTS/decade [23].

ACKNOWLEDGEMENTS

REFERENCES

1. S. S. Wang and D. W. Fitting (Eds.), Composite Materials for Offshore Operations, Proc. 1st International Workshop, National Institute of Standards and Technology, Special Publication 887, 1995.

2. H. Saadatmanesh and M. R. Ehsani (Eds.), Proc. 2nd International Conference on Composites in Infrastructure, ICCI 98, Tucson, AZ, 1998.

3. Bor Z. Jang, Advanced Polymer Composites: Principles and Applications. ASM International, Materials Park, OH, 1994.

4. R. Talreja, Fatigue of Composite Materials, Technomic Publishing Company, Inc., Lancaster, PA, 1987.

5. R. Martin (Ed.), Composite Materials: Fatigue and Fracture, ASTM STP 1230, American Society for Testing and Materials, Philadelphia, PA, 1995.

6. K. L. Reifsnider (Ed.), Fatigue of Composite Materials, Composite Materials Series, Elsevier, Amsterdam, Vol. 4, 1991.

7. K. L. Reifsnider (Ed.), Damage in Composites, ASTM STP 775 , American Society for Testing and Materials, Philadelphia, PA, 1979.

8. P. Chiou and W. L. Bradley, Composites, 26, 869 (1995).

9. C. J. Jones, R. F. Dickson, T. Adam, H. Reiter, and B. Harris, Composites, p.288, July, 1983.

10. M. Watanabe, ASTM STP 674, S. W. Tsai (Ed.), 1970, p.345.

11. K. Komai, K. Minoshima, and S. Shiroshita, Materials Sci. Eng. A143, 155 (1991).

12. R. Adimi, H. Rahman, B. Benmokrane, and K. Kobayashi, Proc. 2nd International Conference on Composites in Infrastructure, H. Saadatmanesh and M. R. Ehsani (Eds.), ICCI 98, Tucson, AZ, 1998.

13. K. E. Hofer, G. N. Skaper, L.C. Bennett, and N. Rao, J. Reinforced Plastics and Composites, 6, 53 (1987).

14. G. S. Springer, B. A. Sanders and R. W. Tung, J. of Composite Materials, 14, 213(1980).

15. A. Plumtree and G. Shen, 8th International Conference on Composite Materials, Vol. 4, 1991, p.1.

16.   Lin Ye, Composites Sci. and Technol., 36, 339 (1989).

17.   Ken Ashbee, Fundamental Principles of Fiber Reinforced Composites. Technomic Publishing Company, Lancaster, PA, 1993.

18.   K. L. Reifsnider, Polymer, 35, 5035 (1994).

19.   S. Subramanian, K. L. Reifsnider, and W. W. Stinchcomb, Int. Journal of Fatigue, 17, No.5, 343 (1995).

20.   C. H Shen and G.S. Springer, J. Composites Materials, 10, 2 (1976).

21.   J. W. Chin, T. Nguyen, and K Aouadi, J. Appl. Polym. Sci. 71, 483 (1999).

22.   L.J. Broutman and S. Sahu, Composite Materials: Testing and Design, ASTM STP 497, 1970, p.170.

23.   P. R. Bevington and D. K. Robinson, Data Reduction and Error Analysis for the Physical Sciences, McGraw-Hill, New York, 1992.

24.   J. Mandell, D. Huang and F.J. McGarry, Proc. 35th Tech Conference on Reinforced Plastics, SPI, 1980, Paper 19-A.

25.   J.J. Lesko, et al., Progress in Durability Analyses of Composite Systems, DURACOSYS '97.

26.   C.L. McKinnis, Fracture Mechanics of Ceramics: Crack Growth and Microstructure, Vol. 4, 1977, p.581.

27.   J. J. Dlubac, G. F. Lee, J. V. Duffy, R. J. Deigan, and J. D. Lee, Sound and Vibration Damping with Polymers, R. C. Corsaro and L. H. Sperling (Eds), ACS Symposium Series 424, 1990, p.49.

28.   P. T. Weissman and R. P. Chartoff, Sound and Vibration Damping with Polymers, R. C. Corsaro and L. H. Sperling (Eds.), ACS Symposium Series 424, 1990, p.111.

29.   J. Mandell and Urs Meier, Long Term Behavior of Composites, ASTM STP 813, T. K. O'Brien (Ed.), American Society for Testing Materials, Philadelphia, PA, 1983.

30.   C. T. Sun and W. S. Chan, Composite Materials, Testing and Design ASTM STP 674, S. W. Tsai (Ed.), American Society for Testing and Materials, Philadelphia, 1979, p.418.

NIST Technical Publications

Periodical

Journal of Research of the National Institute of Standards and Technology—Reports NIST research and development in those disciplines of the physical and engineering sciences in which the Institute is active. These include physics, chemistry, engineering, mathematics, and computer sciences. Papers cover a broad range of subjects, with major emphasis on measurement methodology and the basic technology underlying standardization. Also included from time to time are survey articles on topics closely related to the Institute's technical and scientific programs. Issued six times a year.

Nonperiodicals

Monographs—Major contributions to the technical literature on various subjects related to the Institute's scientific and technical activities.

Handbooks—Recommended codes of engineering and industrial practice (including safety codes) developed in cooperation with interested industries, professional organizations, and regulatory bodies.

Special Publications—Include proceedings of conferences sponsored by NIST, NIST annual reports, and other special publications appropriate to this grouping such as wall charts, pocket cards, and bibliographies.

National Standard Reference Data Series—Provides quantitative data on the physical and chemical properties of materials, compiled from the world's literature and critically evaluated. Developed under a worldwide program coordinated by NIST under the authority of the National Standard Data Act (Public Law 90-396). NOTE: The Journal of Physical and Chemical Reference Data (JPCRD) is published bimonthly for NIST by the American Chemical Society (ACS) and the American Institute of Physics (AIP). Subscriptions, reprints, and supplements are available from ACS, 1155 Sixteenth St., NW, Washington, DC 20056.

Building Science Series—Disseminates technical information developed at the Institute on building materials, components, systems, and whole structures. The series presents research results, test methods, and performance criteria related to the structural and environmental functions and the durability and safety characteristics of building elements and systems.

Technical Notes—Studies or reports which are complete in themselves but restrictive in their treatment of a subject. Analogous to monographs but not so comprehensive in scope or definitive in treatment of the subject area. Often serve as a vehicle for final reports of work performed at NIST under the sponsorship of other government agencies.

Voluntary Product Standards—Developed under procedures published by the Department of Commerce in Part 10, Title 15, of the Code of Federal Regulations. The standards establish nationally recognized requirements for products, and provide all concerned interests with a basis for common understanding of the characteristics of the products. NIST administers this program in support of the efforts of private-sector standardizing organizations.

Order the following NIST publications—FIPS and NISTIRs—from the National Technical Information Service, Springfield, VA 22161.

Federal Information Processing Standards Publications (FIPS PUB)—Publications in this series collectively constitute the Federal Information Processing Standards Register. The Register serves as the official source of information in the Federal Government regarding standards issued by NIST pursuant to the Federal Property and Administrative Services Act of 1949 as amended, Public Law 89-306 (79 Stat. 1127), and as implemented by Executive Order 11717 (38 FR 12315, dated May 11, 1973) and Part 6 of Title 15 CFR (Code of Federal Regulations).

NIST Interagency or Internal Reports (NISTIR)—The series includes interim or final reports on work performed by NIST for outside sponsors (both government and nongovernment). In general, initial distribution is handled by the sponsor; public distribution is handled by sales through the National Technical Information Service, Springfield, VA 22161, in hard copy, electronic media, or microfiche form. NISTIR's may also report results of NIST projects of transitory or limited interest, including those that will be published subsequently in more comprehensive form.